



Proceedings of the Sixth International Conference on
Railway Technology: Research, Development and Maintenance
Edited by: J. Pombo
Civil-Comp Conferences, Volume 7, Paper 21.4
Civil-Comp Press, Edinburgh, United Kingdom, 2024
ISSN: 2753-3239, doi: 10.4203/ccc.7.21.4
©Civil-Comp Ltd, Edinburgh, UK, 2024

Virtually Coupled Trains Dynamics and Energy Efficiency: A Simulation-Based Analysis

R. Parise¹ and K. Mullankuzhy²

¹ Institute of Vehicle Concepts, German Aerospace Center,
Berlin, Germany

² Institute of Vehicle Concepts, German Aerospace Center,
Stuttgart, Germany

Abstract

This paper focuses on virtually coupled train sets, a novel approach to enhancing railway network capacity and efficiency by allowing trains to drive coordinately closer than the absolute brake distance from each other. A simulation tool is developed to analyze the driving behavior of coupled trains, including the coupling and decoupling maneuvers, enabling a detailed study of coupling dynamics. Our investigation extends to the energy consumption relationship between leading and following trains under the influence of stochastic variables such as wind and rolling resistance, alongside an evaluation of the gap control parameters' sensitivity. The findings indicate that while wind gusts moderately increase energy consumption, rolling resistance variability has a negligible effect. Employing sliding mode control with adaptive time headway seems a suitable control choice, highlighting a trade-off between control precision and energy efficiency.

Keywords: virtually coupled train sets, railway network capacity, energy efficiency, simulation tool, coupling maneuvers, stochastic variables, sliding mode control, adaptive time headway, control optimization

1 Introduction

The demand for public transport has escalated rapidly over the years. Building new infrastructure to accommodate more services poses financial and environmental challenges. Therefore, the railway industry is looking for solutions to sustainably expand the capacity of existing railway networks. The adoption of moving block signalling (MBS) system in European Train Control System (ETCS) Level 3 is a step in this direction. However, MBS relies on very conservative assumptions for spacing trains. It uses absolute braking distance (ABD) for spacing trains. Therefore, there is room for further optimization by reducing safe distance maintained by trains. This paves way for the concept of virtually coupled train sets (VCTS).

VCTS aims to change the safe distance paradigm from ABD to relative braking distance (RBD) [1] and thereby increase track capacity. In VCTS two or more trains are electronically connected to each other to form a platoon [2]. Train-to-train communication, relative positioning and advanced train control techniques are used to provide each train awareness of its own characteristics and environment which enable trains to calculate and manage a safe distance from each other and coordinate their movements to form a platoon.

Since trains are virtually connected without using traditional mechanical links, several possibilities for new rail operations open up. For example, trains sharing a route can couple to form platoons, freeing up track space to accommodate more trains. In [3] a study comparing VCTS and MBS showed significant capacity improvements, with VCTS reducing safe distances by 43% compared to MBS. Additionally, VCTS enables trains to couple while moving, saving time and labor compared to mechanical coupling and improving schedule robustness due to enhanced flexibility.

VCTS operations also have energy implications. Energy consumption and its optimization is a crucial aspect that needs to be considered for sustainable railway operations. Several studies have been done on speed profiling for the energy consumption of trains. [4] provides an overview of train speed profiling solutions for optimizing energy consumption. The authors indicate that the energy efficiency of running a single train can only be improved in terms of coasting, as previously studied in [5]. On the other hand, the authors of [6] point to traffic fluidity as one criterion that is relevant for the evaluation of the quality of rail transport services and directly translates into the energy efficiency of train running. In [7] the energy implications of interference with leader train on follower trains when driving under MBS and VCTS with a minimum gap of 2 km were analyzed.

The investigation in this paper extends to the energy consumption relationship between leading and following trains in a VCTS when the leading train is following an energy-optimized trajectory. The influence of stochastic variables such as wind and rolling resistance is analyzed, alongside an evaluation of the gap control parameters' sensitivity.

2 Methods

For this research, a train simulation tool using the programming language Python was developed. This tool was designed primarily to study virtual coupling and analyze the performance of the coupling stability and energy consumption.

Trains in the simulation can be either driving independently and following a pre-calculated target trajectory (Section 2.1) using a trajectory following control (Section 2.2), or as part of a platoon, in which case the train will try to maintain a targeted gap distance using a gap control (Section 2.4). The coupling procedure is described in Section 2.3. With the target force from the controllers, a dynamic model calculates the resistance force using the Davis Equations, while allowing for some variables to be stochastic (Section 2.5). With the resultant force, the simulator uses an Euler method to integrate the speed numerically and the trapezoidal rule for updating the position.

2.1 Optimal Trajectory Generation

The optimal trajectory is calculated using the method developed in [8] for electric trains and later further modified to allow the optimization of the trajectories of hybrid trains [9].

The trajectory optimization takes into consideration the gradient of the tracks, as well as the increase of rolling resistance due to curves. The timetables and maximal speeds serve as boundary conditions. The train resistance is modelled using the Davis equation, and the efficiency curves of internal components such as motors, inverters, and transformers are taken into consideration as well.

2.2 Trajectory Following Control

The optimized trajectory is calculated beforehand and loaded in each train. When trains are driving independently or as leaders in the platoon, a multivariable feedback control (MFC) is used to follow the trajectory using the following equation:

$$u(t) = k_1 \cdot (a_{opt}(t) - a_{actual}(t)) + k_2 \cdot (v_{opt}(t) - v_{actual}(t)) + k_3 \cdot (s_{opt}(t) - s_{actual}(t)) \quad (1)$$

Where the variables a , v and s are the acceleration, velocity and position. The $u(t)$ is the control effort, which influences the forces at the wheel F_{wheel} by Equation (13) below. The control parameters $k_{1..3}$ are optimized by minimizing the loss function

which, besides the total energy consumption, includes other penalty terms:

$$\begin{aligned}
J(s_{actual}, v_{actual}, F_{wheel}, k_{1..3}) = & \\
& \int_{t_0}^T F_{wheel}(t) \cdot v_{actual}(t) + c_1 \cdot \max(0, v_{actual}(t) - v_{limit}(t)) + c_2 \cdot P_{stop}(t) dt \\
& + c_3 \cdot \max(0, s_{actual}(T) - s_{opt}(T)) + c_4 \cdot |k| \\
P_{stop}(t) = & \begin{cases} 1, & \text{if } v_{actual}(t) > 0 \text{ and } v_{opt}(t) = 0 \\ 0, & \text{else} \end{cases}
\end{aligned} \tag{2}$$

where $|k|$ denotes the L^2 -norm of the control parameters, and the coefficients $c_{1..4}$ represent the weight of the penalty for respectively exceeding the speed limit, not stopping at the station at the proper time, not finalizing the service at the proper time, and the regularization of the control weights.

2.3 Coupling Procedures and Gap Policy

VCTS has four operational modes: normal driving, coupling, coupled driving, and decoupling. Inside the platoon, trains can play two roles different roles: the trajectory supervisor, which follows the optimal trajectory and sets the pace for the other trains, and the gap supervisor, which adjusts its dynamics to track the gap and velocity of the trajectory supervisor. Each platoon requires one trajectory supervisor. In the simulation all trains have gap controllers and trajectory following controllers and therefore, can take both roles as trajectory supervisor and as gap supervisor.

1. **Normal driving mode:** In the normal driving mode the trains assume a trajectory supervisor role. This means they will use the trajectory controller to follow the optimal trajectory provided.
2. **Coupling mode:** In the coupling mode, communication between trains is initiated to reduce the gap between them and the trains change roles. The follower remains the trajectory supervisor and the leader takes the role of the gap supervisor. The leader will reduce its speed to converge the gap and then synchronize the speed with the follower.
3. **Coupled driving mode:** Once the coupling manoeuvre is over, the roles are swapped. The leader becomes the trajectory supervisor, and the follower becomes the gap supervisor. Then the follower tracks the leaders speed and maintains a safe gap.
4. **Decoupling mode:** For the decoupling maneuver the gap between the trains need to be increased, so that they can go back to operating independently. When

the decoupling mode starts, the roles do not change but the gap supervisor receives a new target gap which is relatively large. So the follower slows down until the new target gap is achieved while the leader continues following the optimal trajectory. Once the target gap is achieved the trains terminate the communication with each other and continue driving in normal driving mode.

Figure 1 shows an example of two trains transitioning through the various operational modes of VCTS. For the coupling and decoupling procedure, it is important to be sure that no train will violate any speed limit to approach or depart from the platoon. Therefore, if trains are already driving at or close to the speed limit, the train in front should reduce its speed to allow for the next train to catch up, and the inverse should happen during decoupling. During the coupling maneuver, since trains are moving towards each other it is also important to limit the maximal allowed relative speed, to minimize potential hazards.

The chosen gap policy is the Constant time headway policy (CTH), in which the distance maintained between the vehicles is proportional to the speed. CTH policy mimics human driving behavior and is the most researched distance policy because string stability can be achieved with simple V2V communication topologies [10].

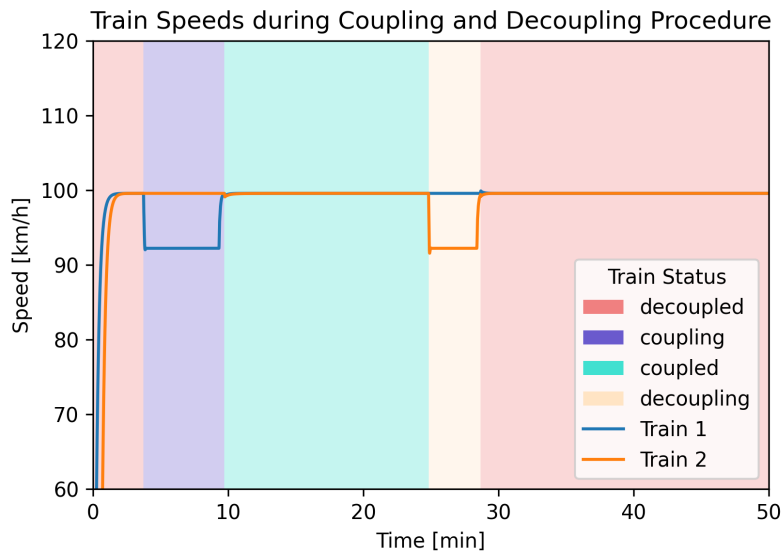


Figure 1: Speed profile of trains during the coupling and decoupling procedures. The approach during coupling is slower due to restriction on the maximal relative speed for a given distance

2.4 Gap Control

For the gap control, when trains are following a leader inside a platoon, a sliding mode controller (SMC) is used. The train responsible for controlling the distance to the leader train receives the states of the leader train and has access to its own state, which are then used to calculate the control effort required $u(t)$. The SMC gap controller is designed by defining a sliding surface that represents the desired system dynamics. This sliding surface incorporates the errors in position e_s and velocity e_v of the follower train relative to the leader train. The communication between trains and sensor accuracy is so far assumed ideal: i.e. no communication loss, delays, or inaccuracies.

The control law used in the sliding mode follows:

$$u(t) = \frac{K \cdot (\sigma(t))}{|(\sigma(t))| + \rho} \quad (3)$$

where K is the controller gain and ρ is the boundary parameter. This control law drives the system in the opposite direction of the error, aiming to eliminate it by bringing the state closer to the surface σ . The boundary layer method is applied to the control signal u to mitigate chattering phenomena, which helps stabilize the control action. Different sliding surfaces are used for the coupled driving mode and the approach maneuver (coupling mode). The latter is separated into two phases, with a third sliding surface with limits the maximal relative speed.

The sliding surface $\sigma(t)$ employed for the coupled driving mode is defined as:

$$\begin{aligned} \sigma(t) &= e_s(t) + \lambda \cdot e_v(t) \\ &= s_{leader}(t) - s_{follower}(t) - t_{target} \cdot v_{follower}(t) + \lambda \cdot (v_{leader}(t) - v_{follower}(t)) \end{aligned} \quad (4)$$

where $e_s(t)$ and $e_v(t)$ are the error in position and velocity w.r.t the leader train, λ is a gain factor, and t_{target} is the desired gap expressed in time.

For the coupling mode, the SMC uses an Adaptive Time Headway (ATH) method, similar to the method proposed by [11], to smoothly decrease the gap to the desired gap. It aims to prevent excessive overshoot resulting from uncontrolled correction effort and to achieve asymptotic convergence of the gap while limiting the relative speed.

This method divides the approach maneuver into two phases. During phase 1, the sliding surface σ_1 is expressed as:

$$\sigma_1(t) = e_s(t) - (t_{carrot}(t) \cdot v_{actual}(t)) \quad (5)$$

To guarantee a smooth transition from the ABD to RBD, the sliding surface is manipulated using an additional carrot headway $t_{carrot} > t_{target}$. The t_{carrot} is initialized

at t_0 (when the coupling procedure starts) as the difference between the current headway and the target one so that the gap control is initialized inside the sliding surface with zero error. Then the carrot headway is asymptotically reduced to zero to achieve the target gap smoothly. The rate at which the carrot headway is reduced in phase 1 is as follows:

$$\begin{aligned} t_{carrot}(t_0) &= \frac{e_s(t_0)}{v_{actual}(t_0)} \\ t_{carrot}(t + \Delta t) &= t_{carrot}(t) - \frac{k \cdot t_{critical} \cdot \Delta t}{v_{actual}(t)} \end{aligned} \quad (6)$$

The rate at which t_{carrot} is reduced is determined by the parameter k and $t_{critical}$. The parameter $t_{critical}$ influences when the control will move from phase 1 to phase 2. Furthermore, the rate at which the t_{carrot} is reduced is also inversely proportional to the actual speed of the train. This means with the increasing speed of the train, the rate at which the gap is converged is slowed down.

Once the follower train reaches the specified headway $\frac{s_{leader}(t) - s_{follower}(t)}{v_{follower}(t)} = t_{critical}$, phase 2 begins. In this phase, a different sliding surface is utilized to facilitate smooth asymptotic convergence to the final desired gap. In phase 2, the sliding surface σ_2 is:

$$\sigma_2 = e_s(t) - t_{carrot}(t) \cdot v_{actual}(t) + (t_{critical} - t_{carrot}(t)) \cdot e_v(t) \quad (7)$$

The difference between the sliding surface σ_1 and σ_2 is that σ_2 also takes into account the the relative speed e_v . This enables more precise control and asymptotic gap convergence. The rate at which the carrot headway is reduced in phase 2 is:

$$t_{carrot}(t + \Delta t) = t_{carrot}(t) - t_{carrot}(t) \cdot \frac{K \cdot \Delta t}{v_{actual}(t)} \quad (8)$$

Furthermore, in order to limit the relative velocity between the trains, a third sliding surface σ_3 is enabled at any point during the approach if the relative velocity exceeds a specified limit $v_{rel,max}$:

$$\begin{aligned} \sigma_3(t) &= v_{leader}(t) - v_{follower}(t) - v_{rel,max}(t) \\ \text{if } |v_{leader}(t) - v_{follower}(t)| &> v_{rel,max} \end{aligned} \quad (9)$$

which effectively limits the relative speed to $v_{rel,max}$.

2.5 Stochastic Variables and Dynamic Model

To accurately model the stochastic influences of environmental and mechanical factors, such as wind resistance and rolling resistance variations, our approach incorporates Gaussian noise processed through a low-pass filter. This methodology is detailed

below, where Δt denotes the simulation time step and L represents the characteristic length:

1. **Gaussian Noise Generation:** At each time t , a random variable n , is sampled from a Gaussian distribution:

$$n \sim \mathcal{N}\left(\mu, \sqrt{\frac{L}{\Delta t}}\sigma\right) \quad (10)$$

where σ is the variance, adjusted by the factor $\sqrt{\frac{L}{\Delta t}}$ to normalize the noise magnitude relative to the time step and characteristic length.

2. **Low-Pass Filtering:** To simulate temporal correlation and smooth transitions, a first-order low-pass filter is applied:

$$f(t) = \alpha \cdot n + (1 - \alpha) \cdot f(t - \Delta t) \quad (11)$$

with $f(t)$ representing the filtered noise at time t . This filter introduces the necessary temporal coherence and smoothness to the noise sequence. Where $\alpha = \frac{\Delta t}{\Delta t + L}$ is defined as the smoothing factor, which controls the degree of correlation between successive noise values.

The characteristic length L encapsulates relevant physical or temporal scales. The normalization of the noise magnitude and α ensures consistent model behavior across varying time steps, crucial for the model's accuracy and scalability. For modeling the wind, the noise signal $f_{wind}(t)$ represents the wind speed. The mean value of the noise μ_{wind} is the average headwind expected by the train, the variance σ_{wind} is the wind gust intensity, and the characteristic length L_{wind} is the gust temporal duration. As seen in the Figure 2.

As for the rolling resistance, the noise signal $f_{roll}(t)$ is a factor by which the resistance will be multiplied (see Equation (13)), which depends on its mean value μ_{roll} and variance σ_{roll} and the characteristic length L_{roll} , which is the spatial scale over which track conditions vary.

The resultant force is calculated as follows:

$$\begin{aligned} F_{resultant}(t) &= F_{wheel}(t) - F_{resistance}(t) \\ &= F_{wheel}(t) - (A + B \cdot v_{actual}(t)) \cdot (1 + f_{roll}(t)) - \\ &\quad C \cdot (v_{actual}(t) + f_{wind}(t))^2 \end{aligned} \quad (12)$$

Where $f_{wind}(t)$ and $f_{roll}(t)$ are the filtered noise given by Equations (10) and (11), and the terms A , B and C are the Davis coefficient [12]. The force at the wheels is a

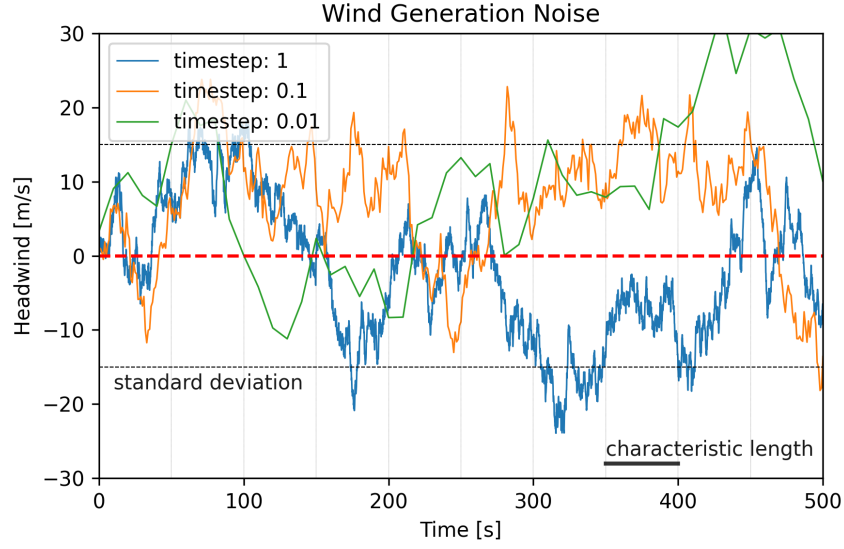


Figure 2: Example noise generation for the wind parameters with a mean (headway) of 0/s and wind gust speed (variance) and duration (characteristic length) of 15m/s and 50 seconds, for different simulation step sizes

function of the control effort $u(t)$ with a first-order delay, give by Equation (13):

$$F_{wheel}(t) = F_{wheel}(t - \Delta t) + \frac{\min\left(u(t) \cdot F_{max}, \frac{P_{max}}{v_{actual}(t)}\right) - F_{wheel}(t - \Delta t)}{\tau} \cdot (\Delta t) \quad (13)$$

3 Results

For the analysis the track Hagen-Warburg was chosen. The service Hagen-Warburg-Hagen comprises 34 stations and takes 5 hours to complete (Figure 3). The optimal trajectory is calculated previously using the tool from [8]. The parameters of the trajectory and gap controller were optimized using a genetic algorithm to minimize the cost from Equation (2).

Initially, a mesh independence study was conducted (Figure 4) to assess the optimal step size. For the following analysis, a step size of 0.01 s is used.

3.1 Stochastic Variables Study

Initially, the sensitivity of total energy consumption is analyzed against the amplitude of the wind resistance and uncertainty of the rolling resistance. Each experiment with

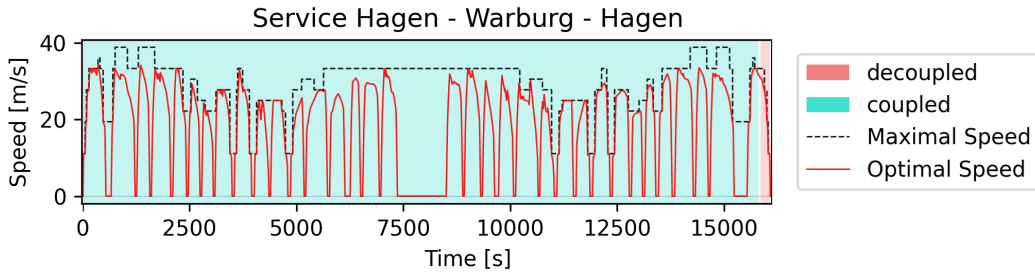


Figure 3: Overview of the service and its optimal trajectory used for the simulation

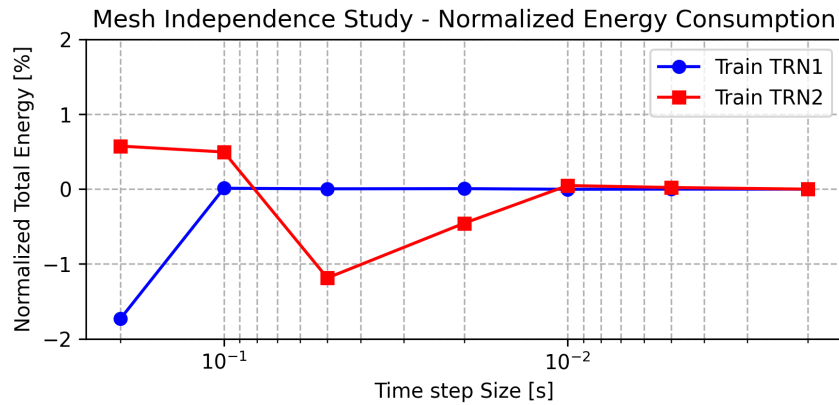


Figure 4: Mesh Independence Study

stochastic variables was repeated 10 times to calculate the mean values and standard deviations.

In Table 1, the standard deviation of the wind noise is set to zero and different mean values are simulated, which is equivalent to a constant headwind.

Wind Speed (km/h)	Leader Energy (MWh)	Follower Energy (MWh)
0.0	776.71 (baseline)	806.36 (baseline)
7.2	793.29 (+2.13%)	822.66 (+2.02%)
14.4	811.24 (+4.45%)	845.94 (+4.91%)
21.6	830.49 (+6.92%)	862.27 (+6.93%)
28.8	851.12 (+9.58%)	882.89 (+9.49%)

Table 1: Headwind Impact on Energy

As expected, the headwind has a quadratic effect on the resistance and is non-negligible for wind already at moderate speeds. However, it is unlikely for the wind to stay constant during the entire trip. Therefore, in Table 2, the average is set to

zero, while different standard deviations of the noise are experimented with, which represent the wind gust intensity.

Wind Gust Speed (km/h)	Leader Energy (MWh) \pm Std	Follower Energy (MWh) \pm Std
14.4	777.52 \pm 5.08 (+0.10%)	808.01 \pm 5.59 (+0.20%)
28.8	781.93 \pm 7.56 (+0.67%)	813.70 \pm 9.34 (+0.91%)
43.2	789.34 \pm 11.21 (+1.63%)	823.30 \pm 11.73 (+2.10%)

Table 2: Wind Gust Impact on Energy

The energy is less impacted by gusts. With a zero mean, it is as likely to encounter gusts in favour and against the driving direction, however, due to the quadratic nature of the resistance force, there is a slight increase in energy consumption at high wind gust speeds. The effect is slightly more pronounced for the follower train, which may be a result of the effort of the gap control tightly regulating the inter-vehicular distance.

As for the rolling resistance, the mean of the noise has a linear impact on the energy consumption, as shown in Table 3. By which is it possible to infer that the rolling resistance corresponds roughly to 20% of the energy expenditure for this service.

Increase in Rolling Resistance (%)	Leader Energy (MWh)	Follower Energy (MWh)
1.0%	778.09 (+0.18%)	807.71 (+0.17%)
2.0%	779.47 (+0.36%)	809.07 (+0.34%)
5.0%	783.62 (+0.89%)	813.16 (+0.84%)
10.0%	790.58 (+1.79%)	829.06 (+2.82%)

Table 3: Rolling Resistance Uncertainty Impact on Energy

Next, the mean of the rolling resistance noise is set to zero and different standard deviations are simulated (Table 4). By the linear nature of the rolling resistance, it can be seen that there is no impact on the leader train. Surprisingly, the energy consumption of the second train also is not impacted, which leads to the conclusion that the gap control does a better job dealing with the rolling resistance noise than the variations in the wind. One reason for this could be the shorter characteristic length chosen for the resistance noise (200 meters), compared to the wind (100 seconds), which might not be enough to disturb the follower train long enough to require corrective measures from the gap control.

Rolling Resistance Standard Deviation (%)	Leader Energy (MWh) \pm Std	Follower Energy (MWh) \pm Std
1.0	776.76 \pm 0.20 (+0.01%)	806.95 \pm 1.73 (+0.07%)
2.0	776.57 \pm 0.56 (-0.02%)	807.32 \pm 2.61 (+0.12%)
5.0	776.34 \pm 0.97 (-0.05%)	806.80 \pm 1.76 (+0.05%)
10.0	777.09 \pm 1.70 (+0.05%)	808.54 \pm 2.50 (+0.27%)

Table 4: Rolling Resistance Noise Impact on Energy

3.2 Gap Control Parameters Study

To analyze the impact of the control parameters on the energy consumption, the base-line scenario was simulated with different boundary parameters ρ and control gains K for the sliding mode control of the gap (Figure 5).

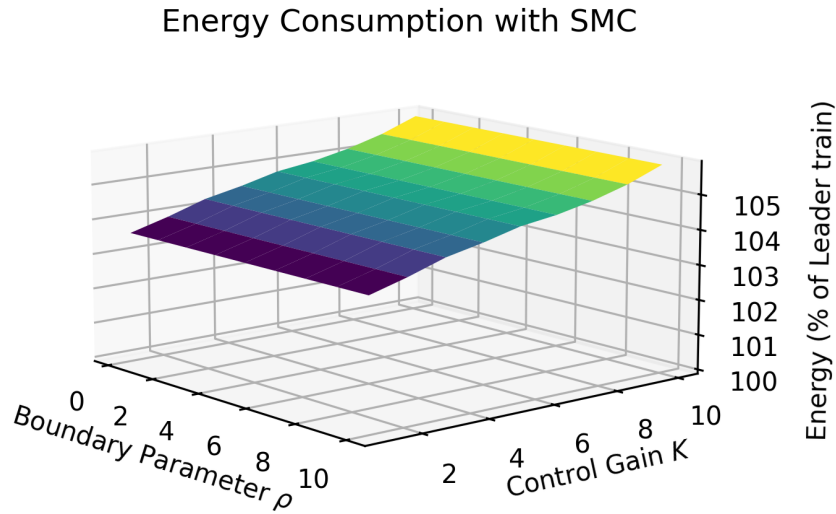


Figure 5: Surface plot of the energy consumption of the follower train for different values of ρ and K parameters of the gap control

The ρ parameter, although important for avoiding chattering, poses little influence on the overall energy consumption, while the control gain K , slightly increases the energy consumption by trying to stay more aggressively on the desired gap. The increase in energy consumption due to a more aggressive control effort likely overshadows the gains of driving close to the optimal trajectory.

4 Conclusions

In conclusion, this study presents an evaluation of the performance of VCTS. Through simulation studies, an analysis of stochastic variables such as wind resistance and rolling resistance reveals that while wind gusts have a moderate impact on energy consumption, the variability in rolling resistance does not significantly affect the energy efficiency of the VCTS system.

Furthermore, the gap control strategy employed in VCTS, particularly the use of SMC with ATH, seems fit to maintain optimal distances between trains even in the presence of noise in the resistance force, ensuring safety and efficiency. The control parameters study underscores the importance of carefully selecting the sliding surface parameters to balance energy consumption and control responsiveness. The results suggest that minimizing deviations from the sliding surface through tighter control may lead to increased energy use, indicating a trade-off between control precision and energy efficiency.

Overall, the adoption of VCTS represents a forward-thinking approach to address the increasing demand for rail transport, offering a scalable solution that enhances capacity and efficiency without the need for extensive infrastructure investments.

References

- [1] B. Ning, "Absolute braking and relative distance braking-train operation control modes in moving block systems," *WIT Transactions on The Built Environment*, vol. 37, 1998.
- [2] J. Winter, A. Lehner, and E. Polisky, "Electronic coupling of next generation trains," in *Proceedings of the Third International Conference on Railway Technology: Research, Development and Maintenance*, vol. 110, Civil-Comp Press, 2016.
- [3] E. Quaglietta and R. Goverde, "Exploring virtual coupling: Operational principles and analysis.," In *Proceedings of the 10th ASPECT Conference of the Institution of Railway Signalling Engineers*, 2019.
- [4] B. Zhang, S. You, L. Zhang, D. Li, and Y. Chen, "Energy-efficient speed profile optimization for high-speed railway considering neutral sections," *IEEE Access*, vol. 9, pp. 25090–25100, 2021.
- [5] W. ShangGuan, X.-H. Yan, B.-G. Cai, and J. Wang, "Multiobjective optimization for train speed trajectory in ctcs high-speed railway with hybrid evolutionary algorithm," *IEEE Transactions on Intelligent Transportation Systems*, vol. 16, no. 4, pp. 2215–2225, 2015.

- [6] E. Koper and A. Kochan, “Testing the smooth driving of a train using a neural network,” *Sustainability*, vol. 12, no. 11, 2020.
- [7] J. Szkopinski and A. Kochan, “Maximization of energy efficiency by synchronizing the speed of trains on a moving block system,” *Energies*, vol. 16, p. 1764, 02 2023.
- [8] M. Schenker, T. Schirmer, and H. Dittus, “Application and improvement of a direct method optimization approach for battery electric railway vehicle operation,” *Proceedings of the Institution of Mechanical Engineers, Part F: Journal of Rail and Rapid Transit*, vol. 235, no. 7, pp. 854–865, 2021.
- [9] F. Kühlkamp, M. Schenker, M. Konrad, and H. Dittus, “Applicability and development of a direct method algorithm for simultaneous optimization of trajectories and energy minimizing control for hybrid fuel cell railway vehicles,” *Proceedings of the Institution of Mechanical Engineers, Part F: Journal of Rail and Rapid Transit*, vol. 237, no. 5, pp. 621–630, 2023.
- [10] K. Massow, I. Radusch, and R. Shorten, “A numerical study on constant spacing policies for starting platoons at oversaturated intersections,” *IEEE Access*, vol. 10, pp. 43766–43786, 2022.
- [11] A. Rupp, M. Steinberger, and M. Horn, “Sliding-mode-based platooning: Theory and applications,” in *Studies in Systems, Decision and Control*, pp. 393–431, Springer International Publishing, 2020.
- [12] E. Fontanel and R. Christeller, eds., *Rolling Stock in the Railway System Vol. 1*. Global Rail Group, 2020.